Shear wave near-surface corrections in the tau-p domain: a case study

Raul Cova, Xiucheng Wei and Kris Innanen

ABSTRACT

Removing near-surface effects in the processing of 3C data is key to exploiting the information provided by converted waves. Receiver-side corrections may need a more accurate approach than source-side corrections due to the complex character of S-wave propagation in the near-surface. In this study a raypath-consistent approach is used to correct the S-wave near-surface effects. This is achieved by transforming the data sorted in receiver gathers to the τ-p domain and performing cross-correlation and convolution operations to capture and subtract the near-surface effects from the data. Results show that this processing improves coherency and stacking power of shallow and deep events simultaneously. Shallow events benefited most from this processing due to their wider range of reflection angles. We also show how the correction of receiver orientations based on reversing the polarity of one of the ends of the spread does not consider receiver stations offset due to obstacles during the acquisition. A full 2D rotation toward the source, as in 3D-3C processing, was applied in this study to account for irregularities in the acquisition geometry.

INTRODUCTION

Removing the near-surface effects from converted-wave seismic data is a critical step in the processing of multicomponent data. Due to the nature of converted-wave propagation, receiver and source corrections are handled differently. Source-side effects can be removed by using near-surface corrections derived from the analysis of refracted P-waves. In contrast, the receiver-side corrections are governed by S-wave velocities and refraction data are usually not available for this wave mode.

Henley (2012) introduced a method to remove S-wave near-surface effects by using interferometric principles applied in the radial-trace (RT) domain. Cova et al. (2014) extended this idea to the τ-p domain, where no assumptions about the velocity model underlying the wave propagation are imposed. An important feature of this method is that near-surface effects are extracted from the reflected data. Therefore, no first break analysis is needed. Moreover, Cova et al. (2014) shows how this methodology accounts for the non-stationary character of the S-wave near-surface effects.

In this report we present a case study in which the near-surface effects were removed by using intereferometric principles in the ray-parameter domain. In contrast to the work presented by Cova et al. (2014) a dataset with fairly complex geology is processed here. We will also show how the pre-processing of the data is an important step, involving at some stages the use of 3D corrections, despite the 2D configuration of the acquisition.

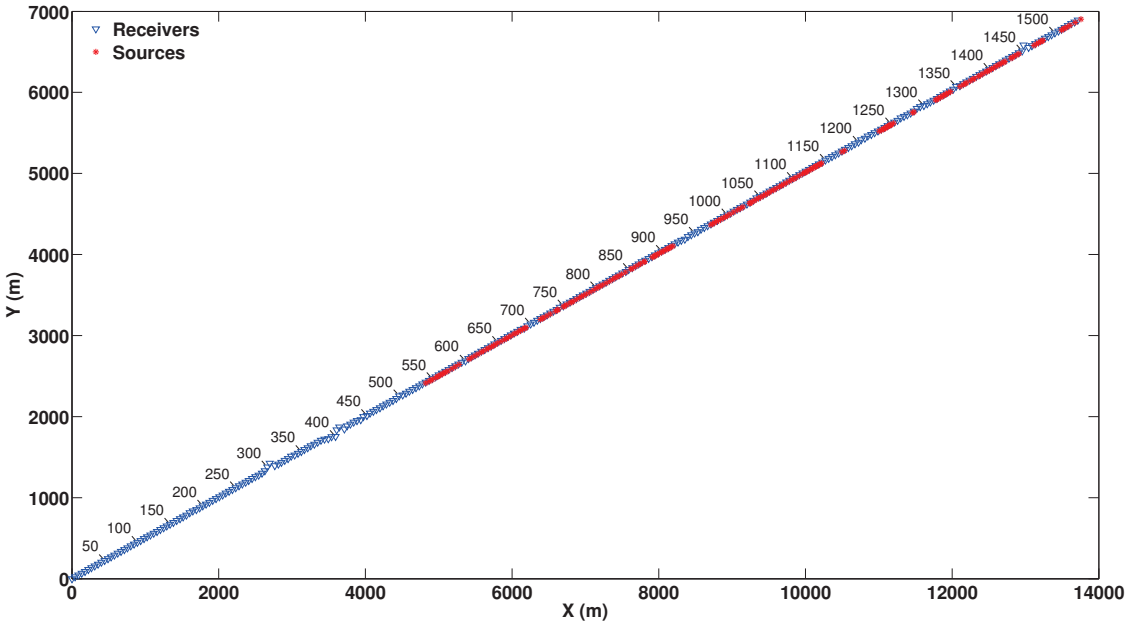

FIG. 1. 2D-3C survey geometry. Notice the presence of gaps in the source locations. No source points were recorded between receiver stations 1 to 540.

DATA PRE-PROCESSING

General description

The data set used in this study consisted of 209 source points with a 20m spacing. A maximum of 1540 channels per shot were recorded with a 10m receiver spacing in a split-spread configuration, providing a maximum offset of 7700m. Figure 1 shows the geometry of the line. Notice that source points start at receiver station 540. This implies that in receiver stations 1 to 500 near-offset information will not be present.

Conventional processing was applied to the vertical component data to produce a reference stack section. Refraction statics were computed after first break picking. This static solution provided the source-side corrections used later in the processing of the horizontal components. Figure 2 shows the resulting CMP stack section. Notice the nearly horizontal and continuous character of the events from CMP 1 to 1000. After CMP 1000, the events show an anticline shape folding.

Rotation toward the source-receiver plane

One of the first steps in the processing of the horizontal components is the rotation of the recorded data into the plane defined by the source and receiver separation and the normal to the measurement surface. The component rotated toward the source is the "radial component" and the perpendicular to it is the "transverse component". In conventional 2D-3C data processing this is achieved by reversing the polarity of all the traces recorded with either positive or negative offsets, depending on the polarity convention chosen by the analyst. This simple correction assumes that all sources and receivers are already located

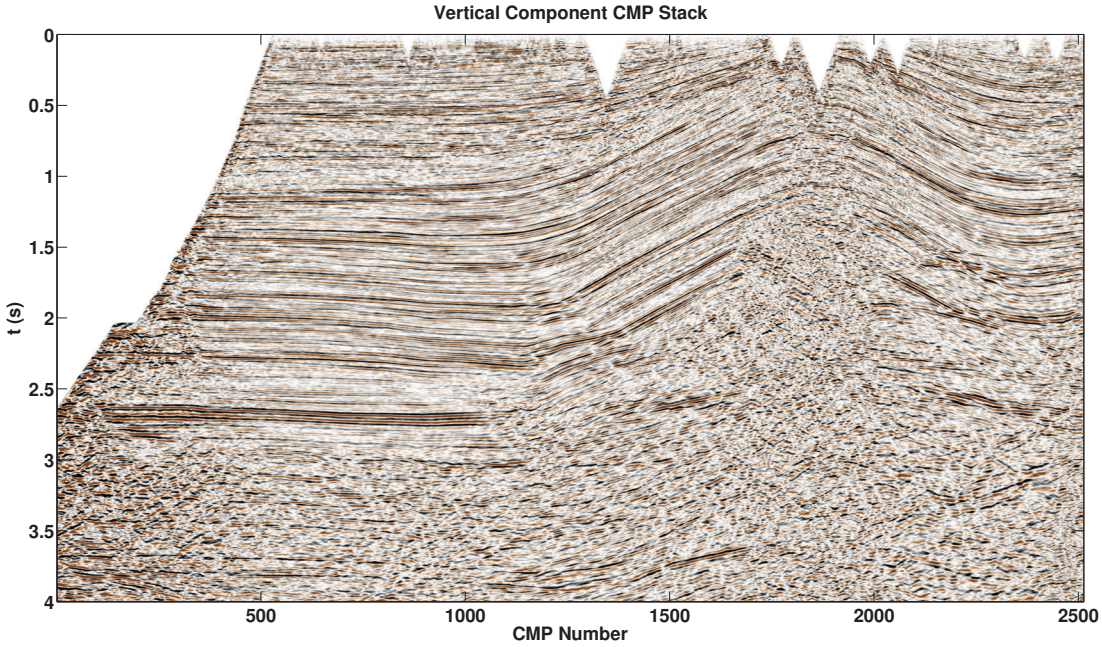

FIG. 2. Vertical component CMP stacked section. Notice the continuity of the events along the line. Reflectors show a flat character between CMP stations 1-1000 and then are folded into an anticline shape.

on the same plane. However, this condition may not be true when obstacles are present on the field and receivers need to be planted outside of the original plane defined by the survey.

Figure 3 shows a zoom around the source station 197 and some of the receivers live for that shot. Notice that the receiver stations 1452-1458 and 1502-1505 are located outside of the original plane define by the 2D survey. A simple polarity reversal will not account for this effect and the rotated data will not represent true radial or traversal components. For this reason, in this study we chose to perform a full 2D rotation as in the processing of 3D-3C data. In this way, the data will be rotated toward the actual plane defined by the source and receiver locations.

Figure 4 (left) shows the inline component data before performing the rotation toward the source. Using the first arrivals of the vertical component data as a reference, we chose to rotate the horizontal components to produce a trough around the first arrivals. In fact, the first arrival energy recorded on the horizontal components is P-wave refracted energy that has been projected onto these components. Based on this, all the traces at positive offsets must show a polarity reversal after rotation, as can be observed in Figure 4 (right). Notice that not only the first arrival energy now shows a consistent polarity but also the low frequency noise displays better coherency.

Since we chose to perform a full 2D rotation, additional changes can be observed on the data recorded at negative offsets. Figure 5 shows a zoom around the first arrivals recorded at negative offsets. Notice how the first arrivals enclosed in the red box show better coherency after rotation. These traces correspond to the receiver stations 1452-1458 which are outside of the original 2D plane defined by the survey. Using a full 2D rotation enabled us to correct

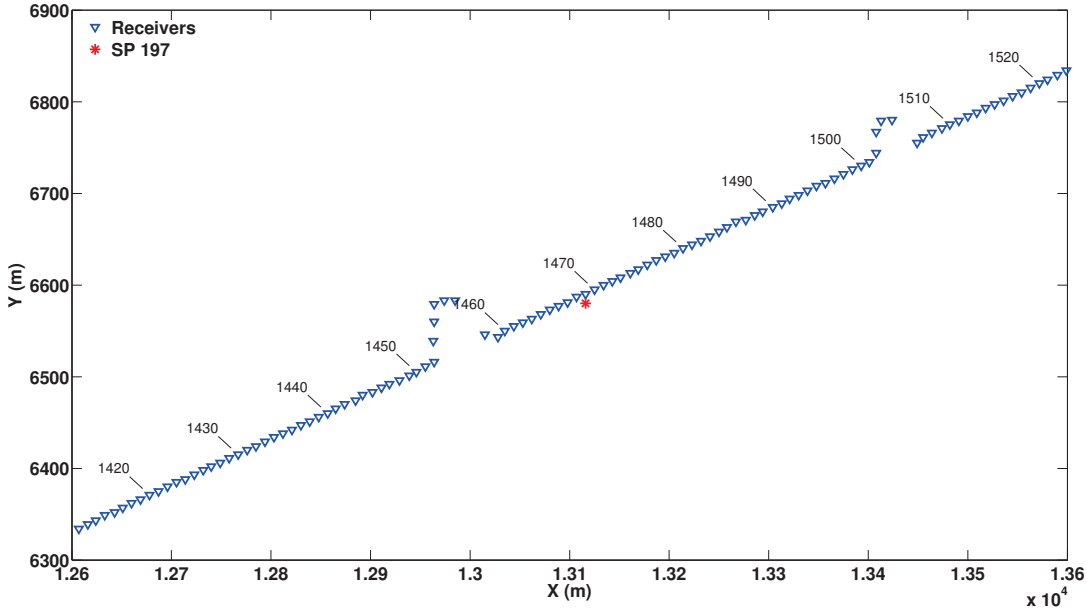

FIG. 3. Receivers used to record source point 197. Notice how the receiver stations 1452-1458 and 1502-1505 are located outside the original plane define by the 2D survey.

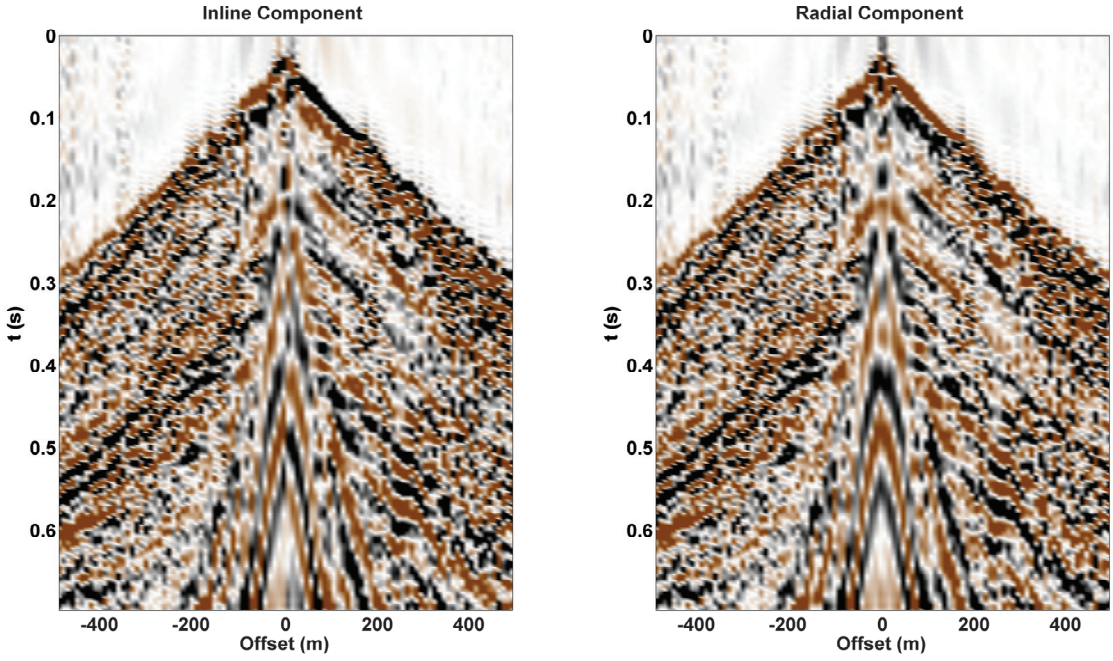

FIG. 4. Source gather 197 before (left) and after (right) rotation toward the radial direction. The polarity of the first arrivals after rotation matches on both ends of the spread. Surface waves signal also displays better coherency.

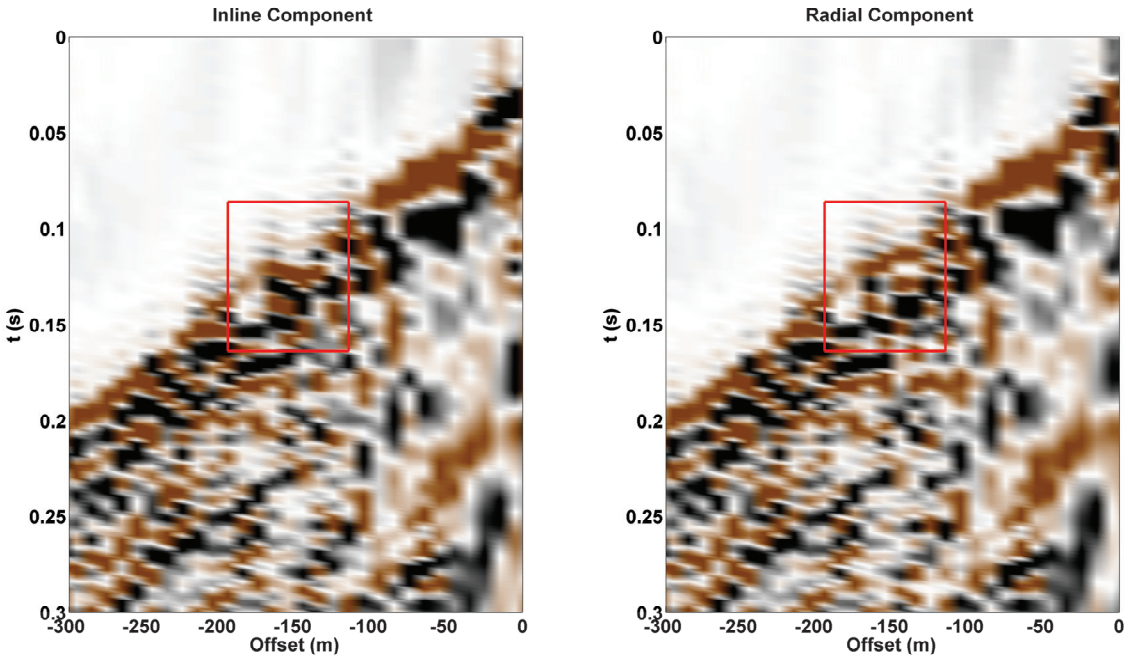

FIG. 5. Zoom view around the first arrivals on the negative offsets of source gather 197. After using a full 2D rotation the first arrivals recorded by the receivers outside of the original 2D plane (red box) show better coherency. This would not have been corrected if a simple polarity reversal on one end of the line was used to rotate the horizontal components toward the source.

for receiver orientation on both ends of the spread and project the data onto true radial and transverse orientations.

Polarity corrections

After rotating the data toward the radial and transverse directions we identified some polarity reversals still present in the data. Figure 6 (right) shows an expanded view of the source point 197 where these polarity reversals are evident. This type of polarity problems may be related to misorientation of the receivers on the field. Comparing the radial and vertical component data (Figure 6, (left)) it can be observed that such polarity reversals are not present on the vertical component data. This confirms that the receivers with polarity reversals were planted with the horizontal components oriented in the opposite direction compared to rest of the survey.

To solve this problem we performed a cross-correlation based analysis to identify all the receiver stations with orientation problems. First, radial and vertical component data were sorted into receiver gathers. Then, the gathers were windowed around the first arrivals, and cross-correlations of the radial and vertical component data were computed. Finally, all the output cross-correlation functions that belong to the same receiver gather were stacked to improve signal/noise ratio. Since the vertical component data is not affected by the misorientation of the horizontal components the output cross-correlation functions must show a change in polarity when compared with neighbour receiver stations.

Figure 7 (top) shows the initial cross-correlation panel for the receiver stations recorded

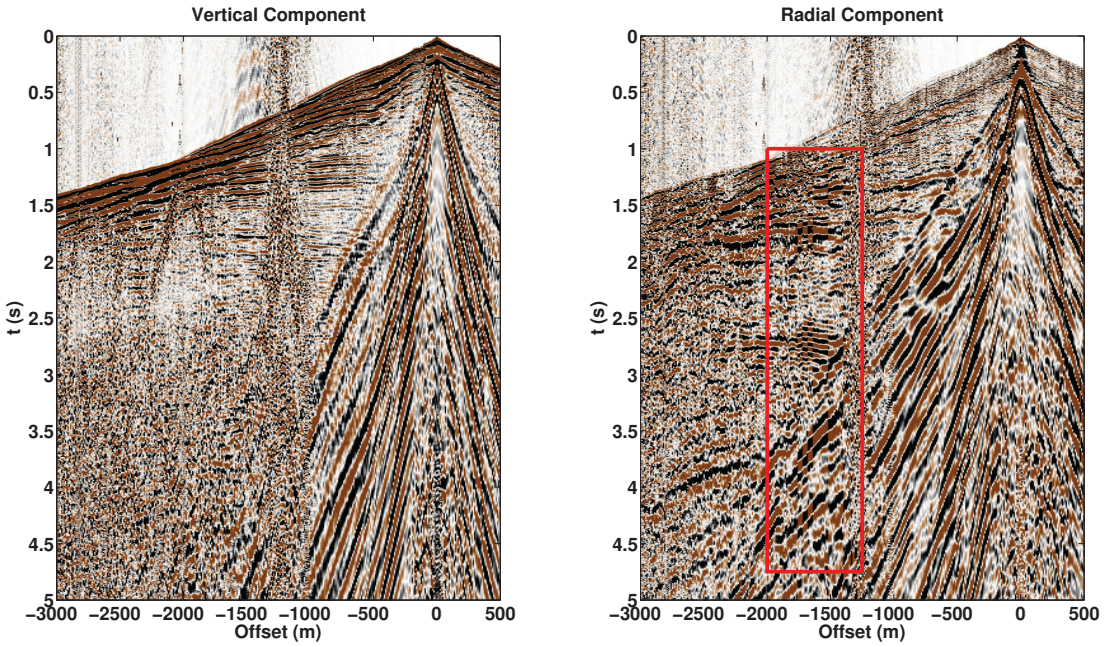

FIG. 6. Vertical (left) and radial (right) component data recorded by source gather 197. Enclosed in the red box is a set of traces with polarity reversal problems.

by source point 197. Notice how the sign of the zero-lag cross-correlation amplitudes changes between receiver stations 1275 to 1350. On this panel the receiver stations with polarity problems can be easily identified and captured.

The previous panel was further improved by performing one additional pass of cross-correlation. In the second pass we created a set of pilot traces which represent the data without polarity reversals. For this purpose we used a wide-window trace-mixing process to remove all the polarity changes, as can be observed in Figure 7 (middle). Next, the initial set of cross-correlation functions are cross-correlated with the pilot functions. The output is shown in Figure 7 (bottom). Notice how the cross-correlation panel now shows shaper amplitudes around the zero-lag of the cross-correlation. To make this correction automatically we captured the sign of the cross-correlation functions at the zero-lag for each receiver stations and save them in our database. This generates a flag with a value of -1 for traces with polarity problems and +1 for traces without problems. These values were loaded to the trace headers and used to remove the polarity reversals by multiplying the traces by these header values.

Figure 8 shows the source gather 197 after polarity corrections. Notice how the events now show a more coherent character. The surface wave noise also displays better coherency which is an important requirement for its effective removal.

NEAR-SURFACE CORRECTIONS

The processing work flow used in this study is based on the ideas presented by Cova et al. (2014) and Henley (2012). In general, this flow consists in moving the data to a raypath-sensitive domain (i.e τ-p, radial traces, etc), building common ray-parameter pan-

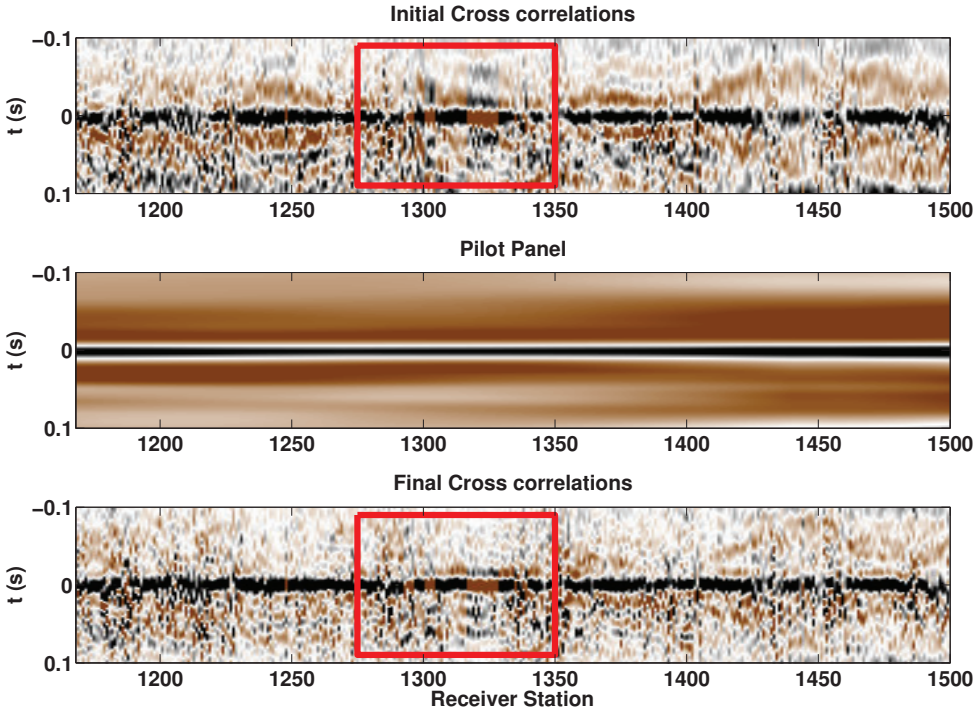

FIG. 7. (top) Vertical and radial components cross-correlation functions stacked by receiver gather. (middle) Pilot traces representing a set of cross-correlation functions without polarity reversal. (bottom) Final set of cross-correlations between the initial set of functions and the pilot panel. Enclosed in the red box the receiver stations with polarity problems can be identified.

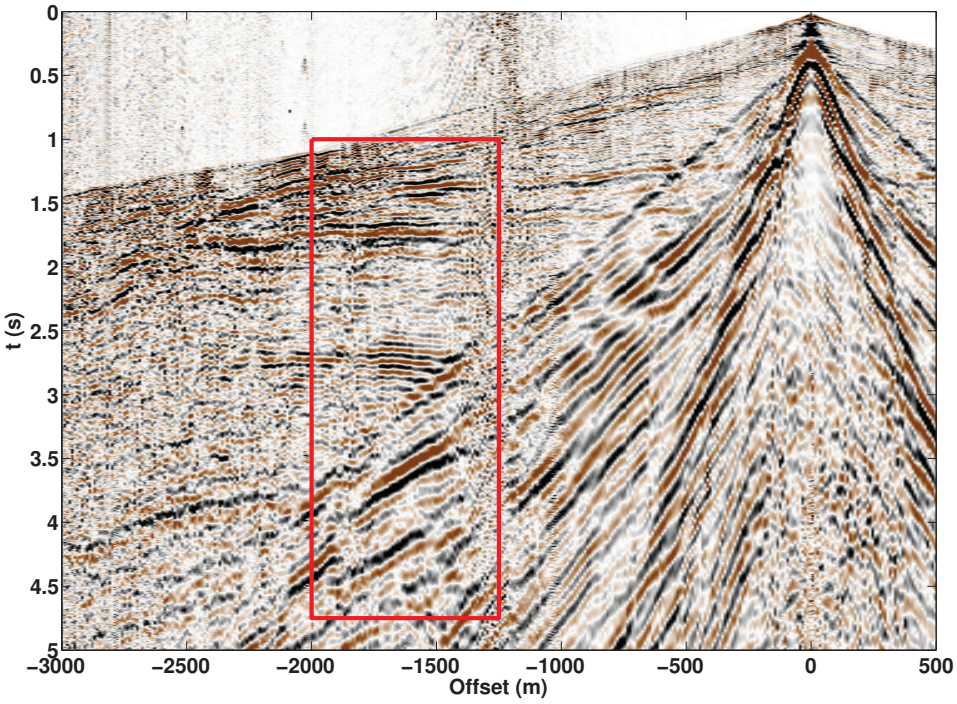

FIG. 8. Source gather 197 after polarity reversals. The events inside the red box now display a consistent polarity.

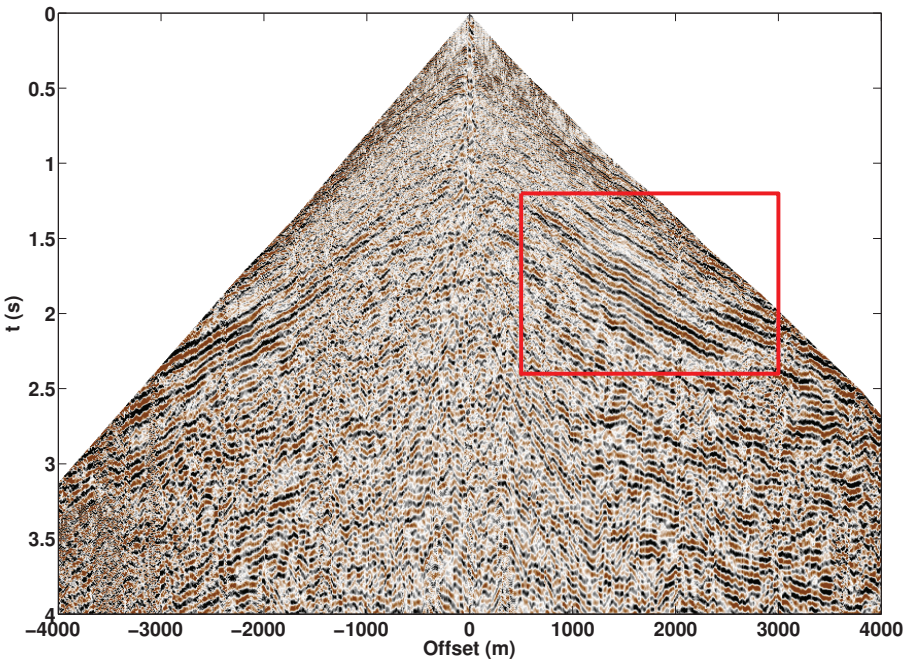

FIG. 9. Source gather 24 after surface waves removal and source static corrections. Notice how the moveout of the events enclosed in the red box are deformed by near-surface effects.

els, computing pilot traces and cross-correlating them with the input data. The output cross-correlation functions should capture the delays caused by the near-surface. Therefore, they can be used as matching filters, which convolved with the original data remove the near-surface effects. After completing these operations the data are returned to their original domain by applying an inverse transformation.

Figure 9 shows a source gather after surface waves removal and source static corrections. Notice how the moveout of the events in the red box is deformed. This type of deformation which seems consistent along the trace is evidence of receiver statics. This can be confirmed by looking at the common receiver stacks sections displayed in Figures 13 (top) and 14 (top). These figures show how the continuity of the events is interrupted by "jumps" that affect the full length of the traces.

The first step in the workflow to remove the near-surface effects is to sort the data into receiver gathers and transform them to the τ-p domain. Figure 10 shows an example of a receiver gather both in x-t (left) and τ-p domain (right). It is important that the parameters chosen for the transformation preserve all the important data originally recorded. For this reason we recommend to apply an inverse transform to the data, before doing any further processing, and check to see whether the original data are fully recovered.

The next step is to sort the data into ray-parameter panels. Figure 11 (top) shows all the traces with a ray-parameter value of -5×10^{-4} recorded at each receiver location. Then, pilot panels are computed by forcing the events to show a continuous character. In this case a horizon that follows the structural trend of the geology was picked and used to flatten the data. Then, a trim static correction and trace-mixing process were applied to remove

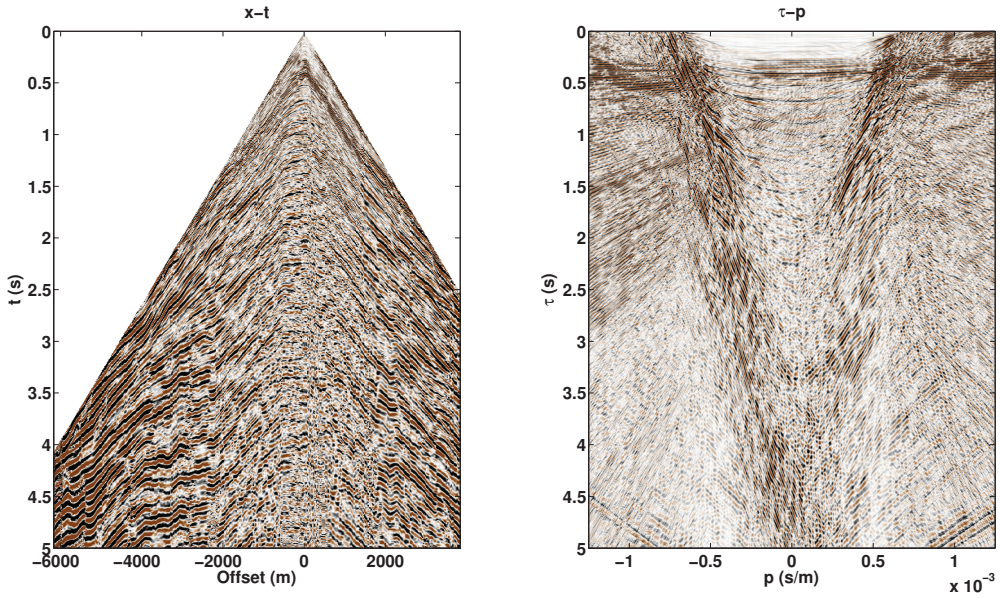

FIG. 10. Receiver gather 924 before (left) and after (right) transformation to the τ-p domain.

any shift between traces and smooth the amplitudes. Finally, the structural trend is added back to the traces. Figure 11 (bottom) shows the pilot panel for the ray-parameter value -5×10^{-4}.

At this point, the principles of traveltime interferometry as defined by Schuster (2005) are invoked. The following steps consist of a series of addition and subtraction of travel times by means of cross-correlation and convolution operations. First, the near-surface effects are captured by cross-correlating the raw ray-parameter panels with the pilot panels. Figure 12 (top) shows the output of this process. The spectrum of this set of cross-correlation functions have been whitened by using a spiking deconvolution. With this step, we seek to produce a set of inverse filters with a wide enough spectrum that preserves the original spectrum of the data during the next step. Finally, the near-surface effects are removed by convolving the raw ray-parameter panels with the set of conditioned cross-correlation functions. The output of this process is shown in Figure 12 (bottom). There we can see how the continuity of the events has been improved by removing the jittering that was present in the data.

After all the ray-parameter panels are corrected, the data is sorted back into receiver gathers and an inverse τ-p tranformation is performed. Figures 13 and 14 display common receiver stacks before and after near-surface corrections. Notice how the events shows better coherency. Moreover, in Figure 14 (bottom) we can observe how on the events above 0.8s not only coherency have been improved but also the seismic resolution.

The observations made on the common receiver stacks also apply to the common conversion point (CCP) stacks in Figures 15 and 16. In these stacked sections spiking deconvolution and FX filters have been applied to improve resolution and coherency of the events. Notice that this type of post-processing does not remove the jittering present in the raw data. Only after removing the near-surface effects, the continuity of the events is dramati-

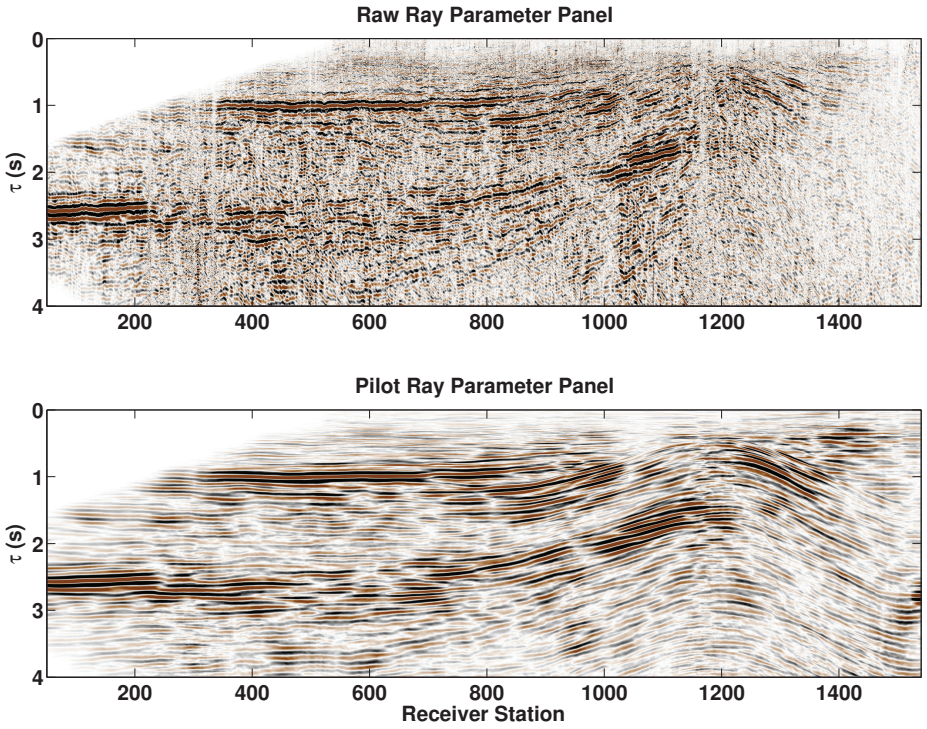

FIG. 11. (top) Ray-parameter panel $p = -5\times10^{-4}$. (bottom) Pilot panel computed for ray-parameter $p = -5 \times 10^{-4}$.

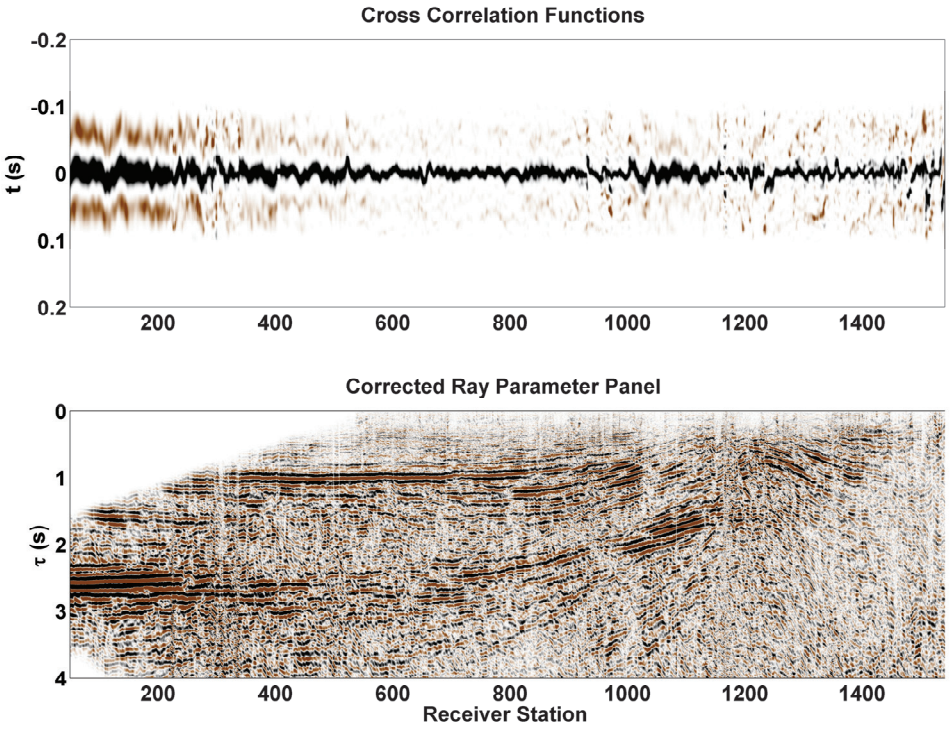

FIG. 12. (top) Cross-correlation functions produced between raw and pilot traces for the ray-parameter $p = -5 \times 10^{-4}$. (bottom) Ray-parameter panel $p = -5 \times 10^{-4}$ after convolution between the raw traces and the set of cross-correlation functions.

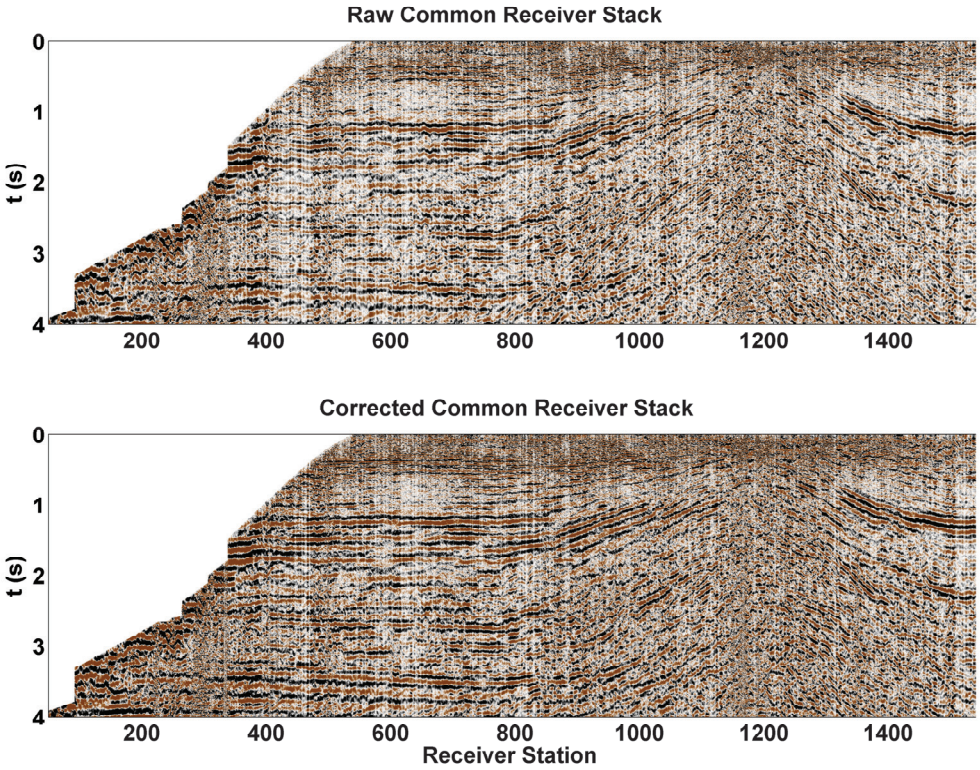

FIG. 13. Common receiver stacked sections before (top) and after (bottom) removing near-surface effects.

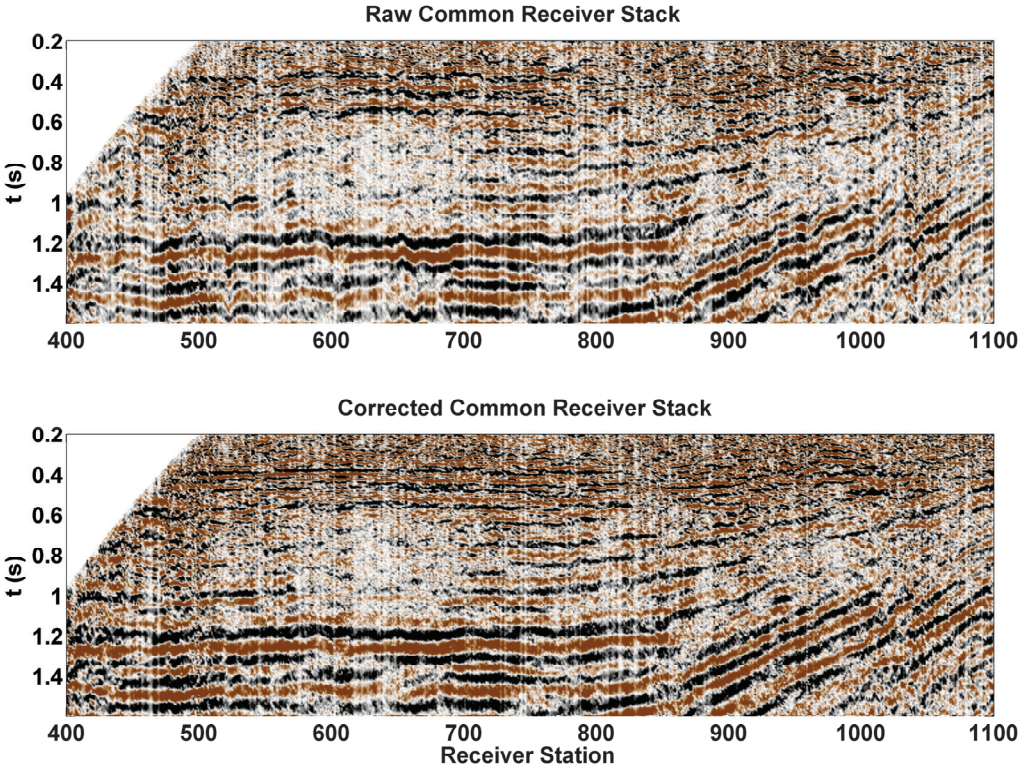

FIG. 14. Zoom view around receiver stations 400-1100 before (top) and after (bottom) removing near-surface effects.

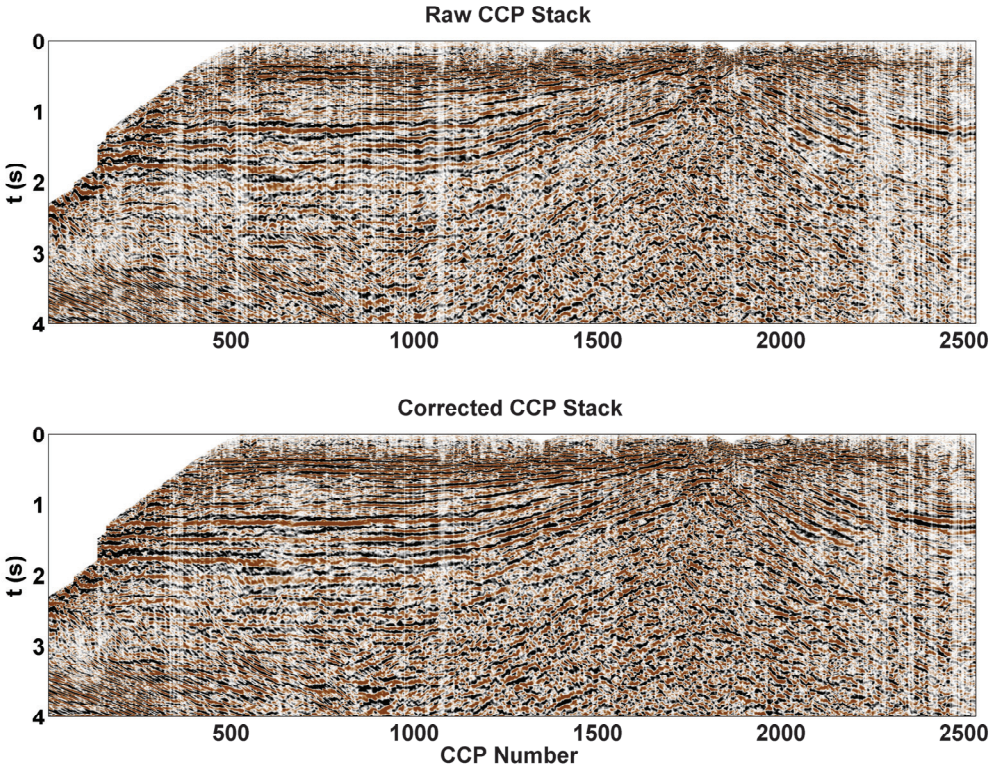

FIG. 15. Common conversion point (CCP) stacked sections before (top) and after (bottom) removing near-surface effects.

cally improved, especially in the shallower part of the section. The reason for this is that, these events are the ones that may experience a wider range of reflection angles. Therefore, they will be the most benefited by removing the near-surface effects in a ray-path consistent framework.

CONCLUSIONS

The simplifications that are generally used in the geometrical rotation of 2D-3C data toward the source-receiver plane may not be enough in some cases. Changing the polarity of the receivers in one end of the spread does not consider the fact that some receivers may be outside of the plane defined by the survey. In this study, a full 2D rotation was needed to properly distribute the recorded amplitudes into the radial and transverse direction.

The ability of raypath-consistent corrections to accommodate near-surface effects for shallow and deep events simultaneously is one of the most important features of this type of processing. In the processing of deep reflection data the assumption of vertical ray-path angles may be sufficient for the use of a surface consistent approach. However, the very low velocity of S-waves and the ability of shallow events to reach wider reflection angles requires a ray-path dependent framework. The methodology we showed in this study demonstrates how this can be achieved even when the geology of the area presents some structural complexity.

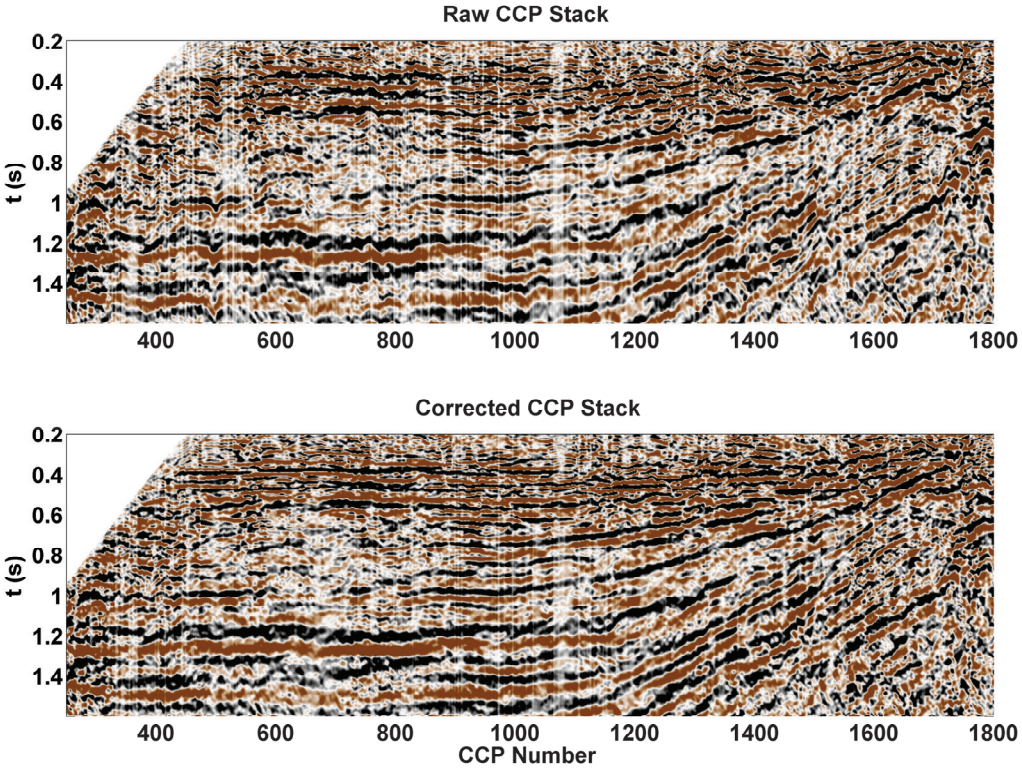

FIG. 16. Zoom view around CCP stations 500-1800 before (top) and after (bottom) removing near-surface effects.

ACKNOWLEDGEMENTS

The authors would like to thank SINOPEC for providing the data and permission to publish these results. This work was funded by CREWES industrial sponsors and NSERC (Natural Science and Engineering Research Council of Canada) through the grant CRDPJ 461179-13. We also thank David Henley for helping in the editing of this report.

REFERENCES

Cova, R., Henley, D., and Innanen, K., 2014, Addressing non-stationary shear wave statics in the rayparameter domain: CREWES Research Report, **26**, 1–17.

Henley, D., 2012, Interferometric application of static corrections: Geophysics, **77**, No. 1, Q1–Q13.

Schuster, G., 2005, Fermats interferometric principle for target-oriented traveltime tomography: Geophysics, **70**, No. 4, U47–U50.